

This document is confidential and is proprietary to the American Chemical Society and its authors. Do not copy or disclose without written permission. If you have received this item in error, notify the sender and delete all copies.

Magnetic bistability in a submonolayer of sublimated Fe₄ Single-Molecule Magnets

Journal:	<i>Nano Letters</i>
Manuscript ID:	Draft
Manuscript Type:	Communication
Date Submitted by the Author:	n/a
Complete List of Authors:	<p>Sessoli, Roberta; University of Florence, Department of Chemistry Malavolti, Luigi; Università degli Studi di Firenze & INSTM RU of Firenze, Dipartimento di Chimica 'Ugo Schiff' Lanzilotto, Valeria; Università degli Studi di Firenze & INSTM RU of Firenze, Dipartimento di Chimica 'Ugo Schiff' Ninova, Silviya; Università degli Studi di Firenze & INSTM RU of Firenze, Dipartimento di Chimica 'Ugo Schiff' Poggini, Lorenzo; Università degli Studi di Firenze & INSTM RU of Firenze, Dipartimento di Chimica 'Ugo Schiff' Cimatti, Irene; Università degli Studi di Firenze & INSTM RU of Firenze, Dipartimento di Chimica 'Ugo Schiff' Cortigiani, Brunetto; Università degli Studi di Firenze & INSTM RU of Firenze, Dipartimento di Chimica 'Ugo Schiff' Margheriti, Ludovica; Università degli Studi di Firenze, Chemistry Chiappe, Daniele; CNR-IMM , Laboratorio MDM Otero, Edwige; Synchrotron Soleil, Totti, Federico; Univeristy of Florence, Chemistry Cornia, Andrea; Università di Modena e Reggio Emilia, Dipartimento di Scienze Chimiche e Geologiche Mannini, Matteo; Università degli Studi di Firenze, Chemistry</p>

SCHOLARONE™
Manuscripts

1
2
3
4
5
6
7
8
9
10
11
12
13
14
15
16
17
18
19
20
21
22
23
24
25
26
27
28
29
30
31
32
33
34
35
36
37
38
39
40
41
42
43
44
45
46
47
48
49
50
51
52
53
54
55
56
57
58
59
60

Magnetic bistability in a submonolayer of sublimated Fe₄ Single-Molecule Magnets

Luigi Malavolti,[†] Valeria Lanzilotto,[†] Silviya Ninova,[†] Lorenzo Poggini,[†] Irene Cimatti,[†]

Brunetto Cortigiani,[†] Ludovica Margheriti,[†] Daniele Chiappe,[‡] Edwige Otero,[§]

Philippe Sainctavit,^{§,£}

Federico Totti,[†] Andrea Cornia,[§] Matteo Mannini,[†] and Roberta Sessoli^{†}*

[†]Department of Chemistry ‘Ugo Schiff’ and INSTM Research Unit, University of Florence,

50019 Sesto Fiorentino, Italy

[‡]Department of Physics, University of Genova, 16146 Genova, Italy

[§]Synchrotron SOLEIL, L’Orme des Merisiers, Saint Aubin BP48 91192 Gif-sur-Yvette Cedex,

France

[£]IMPMC, UMR7590 CNRS, Université Pierre et Marie Curie, MNHN, IRD, 75005 Paris, France

[§]Department of Chemical and Geological Sciences and INSTM Research Unit, University of

Modena and Reggio Emilia, 41125 Modena, Italy

KEYWORDS: Single molecule magnet, scanning tunneling microscopy, X-ray magnetic circular dichroism, density functional theory.

1
2
3 ABSTRACT
4
5
6

7 We demonstrate that Fe₄ molecules can be deposited on gold by thermal sublimation in ultra-
8 high vacuum with retention of single molecule magnet behavior. A magnetic hysteresis
9 comparable to that found in bulk samples is indeed observed when a submonolayer film is
10 studied by X-ray magnetic circular dichroism. Scanning tunneling microscopy evidences the
11 coexistence of Fe₄ molecules assembled in a 2D lattice with short-range hexagonal order and
12 traces of a smaller contaminant. The presence of intact Fe₄ molecules and the retention of their
13 bistable magnetic behavior on the gold surface evidenced by our low temperature synchrotron
14 characterization are supported by density functional theory calculations.
15
16
17
18
19
20
21
22
23
24
25
26

27 Molecules exhibiting magnetic hysteresis, also known as Single Molecule Magnets (SMMs),
28 have been the target of intense research as they represent the ultimate miniaturization limit of
29 magnetic memories, with a profusion of quantum effects governing the dynamics of the
30 magnetization.¹⁻⁴ Recent efforts have focused on the investigation of individual SMMs by either
31 depositing them on a conducting surface and using the lateral resolution of scanning probe
32 techniques⁵⁻⁷ or inserting them in nanojunctions and nanostructures.⁸⁻¹³ The most investigated
33 system is bis(phthalocyaninato)terbium(III) (TbPc₂), a neutral complex characterized by a huge
34 anisotropy barrier for the reversal of the magnetization and a remarkable chemical stability.¹⁴ In
35 the bulk phase, it exhibits a moderately high-temperature hysteresis that was found to persist
36 when deposited on highly oriented pyrolytic graphite^{15,16} or chemisorbed on a silicon surface.¹⁷
37 However, magnetic bistability disappears upon sublimation on metallic surfaces.¹⁸⁻²² Earlier
38 reports focused also on tetrairon(III) (Fe₄) clusters with a propeller-like structure, which display
39 a much weaker anisotropy and sub-kelvin blocking temperatures. Significantly, sulfur-
40
41
42
43
44
45
46
47
48
49
50
51
52
53
54
55
56
57
58
59
60

1
2
3 functionalized complexes of this class retain a molecular hysteresis once chemisorbed as
4 monolayers (MLs) on a gold substrate.^{23,24} Specific Fe₄ derivatives were also found to withstand
5 thermal sublimation; with this procedure, thick films were deposited on a non-conductive
6 substrate and shown to retain slow relaxation of the magnetization.^{25,26} To the best of our
7 knowledge, no magnetic or morphologic characterizations of Fe₄ ultrathin films sublimated on a
8 conductive substrate have been reported yet. Such a statement can be also extended to
9 computational studies on Fe₄ clusters adsorbed on surfaces.

10
11
12
13
14
15
16
17
18
19
20 In this work we have exploited the robustness of Fe₄ SMMs to grow submonolayer films on
21 gold substrates by thermal sublimation. The adsorption of these complex molecules on Au(111)
22 single crystal has been studied by means of scanning tunneling microscopy (STM) in ultra-high-
23 vacuum conditions (UHV). Very low-temperature X-ray Magnetic Circular Dichroism (XMCD)
24 experiments have provided direct access to magnetic behavior, confirming the retention of SMM
25 properties also at submonolayer coverage. These cutting-edge experimental efforts have been
26 flanked by state-of-art structural and magnetic Density Functional Theory (DFT) analysis.
27 Overall, a sound and in-depth picture of the adsorption process as well as of the electronic and
28 magnetic properties of Fe₄ SMMs on gold emerged clearly from the study here presented. The
29 results prove that fully-functional SMMs can be organized in a submonolayer in vacuum
30 conditions, an achievement of relevance for molecular spintronics.

31
32
33
34
35
36
37
38
39
40
41
42
43
44
45
46 The specific derivative herein considered is [Fe₄(L)₂(dpm)₆] (**Fe₄Ph**), where Hdpm is
47 dipivaloylmethane and H₃L is the tripodal ligand 2-hydroxymethyl-1-2-phenylpropane-1,3-diol.
48 The Fe^{III} ions (*s* = 5/2, high spin) adopt a metal centered triangular topology in the structure, as
49 shown in Fig. 1a. Two tripodal ligands, one above and one below the plane of the four Fe^{III} ions,
50 act as bridges and promote an antiferromagnetic interaction between the central spin and the
51
52
53
54
55
56
57
58
59
60

peripheral ones. A ground state with total spin $S = 5$, schematized by the arrows in Fig. 1a, is selectively populated at liquid helium temperature. This family of SMMs is characterized by a moderate uniaxial magnetic anisotropy along the normal (z) to the plane defined by the four metal ions, described in first approximation by the spin Hamiltonian $H_{an} = DS_z^2$; here, S_z is the z -component of the total spin operator for the ground state and $\frac{D}{k_b} \approx -0.6$ K. The potential barrier to be overcome in order to invert the magnetization, given in first approximation by $\Delta E = DS^2$, is thus only 15 K while a hysteresis loop opens only slightly below 1 K.

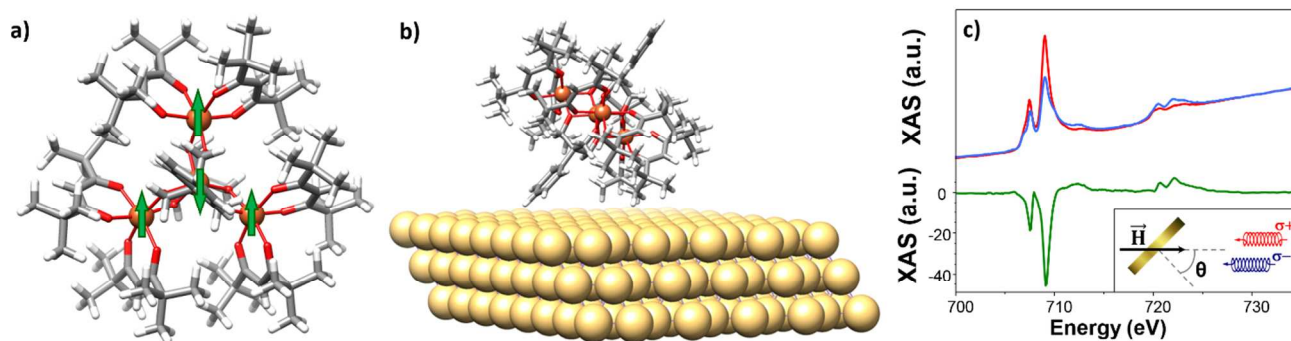


Figure 1: (a) **Fe₄Ph** structure viewed along the idealized C_3 axis, with arrows depicting the arrangement of the Fe^{III} spins in the ground $S = 5$ state; color code: Fe = orange, O = red, C = grey, H = light grey. (b) DFT optimized geometry of the **Fe₄Ph** molecules deposited on Au substrate, showing that the idealized C_3 axis forms an angle of ca. 35° with the normal to the surface. (c) X-ray absorption spectra at the Fe $L_{2,3}$ edges acquired at 0.68 K with 30 kOe field and $\theta = 0^\circ$, where σ^+ and σ^- are the red and blue curves respectively along with the derived XMCD% spectrum in green (see Supporting Information (SI) for details). The scheme reported in the inset of panel (c) shows the setup geometry adopted during the XMCD experiments.

The synthesis of **Fe₄Ph**·Et₂O and the characterization of thermally sublimated thick films were reported earlier.²⁵ In the present study large single crystals of **Fe₄Ph**·Et₂O were crushed and

1
2
3 employed as high purity starting material for deposition of submonolayer films by using an
4 home-made Knudsen cell. Coverage estimation was made by comparing XPS and XAS data with
5 those acquired for a chemisorbed layer of a thioacetyl-substituted Fe₄ SMM on gold which was
6 taken as the monolayer reference (see Supporting Information, SI). As for the XMCD
7 measurements, we referred to XAS signal recorded at the Fe of the iron L₃ edge, while for the *in-*
8 *house* STM investigation the XPS Fe 2*p* / Au 4*f* intensity ratio was used. Moreover, the XPS-
9 based coverage evaluation was further confirmed by STM experiments. Two coverage,
10 corresponding to 0.2 and 0.8 ML, were then selected for the *in-situ* STM characterization. In
11 order to reduce the mobility of the molecules on the surface and improve lateral resolution, the
12 images were acquired by cooling the sample to 30 K; furthermore, a low tunneling current, *i.e.*
13 below 10 pA, was employed in order to prevent damaging of the Fe₄ molecules. The STM
14 images for the 0.2 ML sample are shown in Fig. 2a,b. The **Fe₄Ph** molecules appear to form
15 densely packed islands of approximately spherical objects with average lateral dimensions of *ca.*
16 1.66 ± 0.20 nm (Fig. 2c), which are comparable to those expected for intact **Fe₄Ph** (*ca.* 1.8 nm
17 for the largest dimension)²⁷ based on the optimized structure by DFT calculation (see below and
18 Fig. 2e).

19
20 Along with spherical objects, the sample shows domains with rather different appearance
21 whose internal structure could not be resolved (Fig. S2.1). Their height (0.30 ± 0.05 nm), though
22 determined by STM and therefore convoluted with density of states, suggests that they cannot be
23 associated with Fe₄Ph molecules but rather with smaller units, either contaminants or fragments.
24 We notice that before deposition the pristine material was subject to a long degasing process
25 (several hours at 473 K) in order to eliminate volatile contaminants, such as Et₂O or traces of
26 free ligands. On the other hand, the sublimation and thermal decomposition temperatures of
27
28
29
30
31
32
33
34
35
36
37
38
39
40
41
42
43
44
45
46
47
48
49
50
51
52
53
54
55
56
57
58
59
60

Fe₄Ph (488 K and *ca.* 508 K, respectively) are close to each other, so that a partial decomposition of the **Fe₄Ph** molecule during the sublimation process cannot be ruled out. As an alternative explanation, an on-surface decomposition process may occur, involving reactive sites on the Au(111) substrate.

The contaminant seems to have a high sticking coefficient on the bare gold substrate covering a significant part of it (see Fig. 2a). This result has obvious consequences on the adsorption process of the **Fe₄Ph** molecules. Indeed, the **Fe₄Ph** islands show a broad and asymmetric heights distribution with two different contributions centered at 0.82 ± 0.11 nm and 1.05 ± 0.11 nm, respectively. The difference between the two centers is comparable to the height of the aforementioned contaminant domains, suggesting that a fraction of the **Fe₄Ph** molecules are directly in contact with the gold substrate, while the remaining molecules lie on the contaminants.

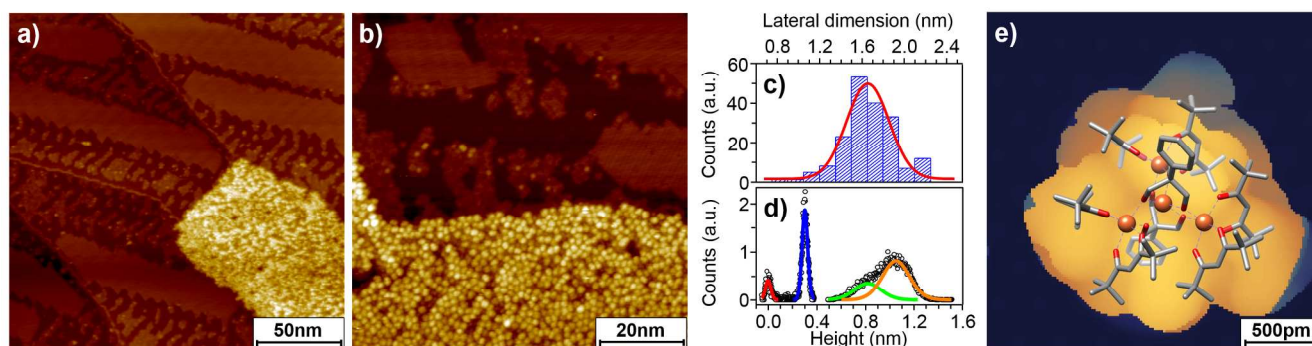
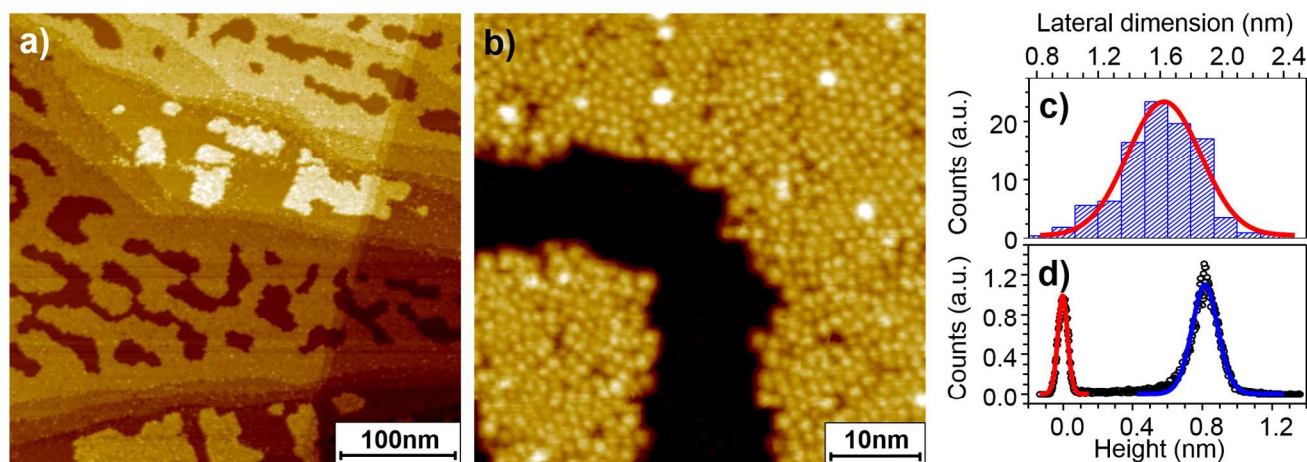


Figure 2. STM images acquired at 30 K for **Fe₄Ph** sublimated on Au(111) single crystal. (a) Large scale image of the 0.2 ML sample (135×135 nm², 3 pA, 2.5 V). (b) Same sample investigated at higher magnification (80×80 nm², 10 pA, 2.0 V). (c) Lateral size distribution of the **Fe₄Ph** molecules extracted from image (b) along with its Gaussian fit. (d) Height distributions in (b) with the red Gaussian reproducing the roughness of the bare gold while the blue one reproduces the height distribution of the contaminants domains; two Gaussian curves

1
2
3 are used to reproduce the broad height distribution associated to the **Fe₄Ph** molecules (green and
4 orange lines). (e) Calculated STM image of **Fe₄Ph** adsorbed on Au(111) at 2 V bias (occupied
5 states), superimposed on the DFT-optimized structure.
6
7
8
9

10
11
12
13
14 Increasing the coverage to *ca.* 0.8 ML a slightly different situation is observed. The large scale
15 image (Fig. 3a) shows the presence of a homogeneous first layer which is characterized by the
16 presence of few second-layer islands and meandering hollows. Within the first layer, the
17 molecules tend to spread forming an almost complete single layer suggesting a quasi layer-by-
18 layer growth of the molecular film. As shown in Fig. 3b the molecules of dimension 1.63 ± 0.24
19 nm (Fig. 3c) are organized in densely packed domains with short range hexagonal order. At this
20 coverage the contaminants domain cannot be identified. It is interesting to notice that a unique
21 height distribution is detected, centered at 0.82 ± 0.12 nm (see Fig.3d), thus practically identical
22 to one of the two contributions observed for the 0.2 ML coverage. A similar height is estimated
23 for the second layer (0.96 ± 0.13 nm, see Fig. S2.2in SI). It is therefore impossible to assess if,
24 for higher coverages, the **Fe₄Ph** molecules are deposited directly on gold or on a full monolayer
25 of contaminants.
26
27
28
29
30
31
32
33
34
35
36
37
38
39
40
41



1
2
3 **Figure 3.** (a) STM image of the 0.8 ML sublimated sample of **Fe₄Ph** (389×389 nm², 10 pA, 2.0
4 V). (b) Enlarged view of the same surface (50×50 nm², 10 pA, 2.0 V). (c) Lateral size
5 distribution of the **Fe₄Ph** molecules extracted from image (b) along with its Gaussian fit. (d)
6 Height distributions in (b) with the red and blue Gaussian fits reproducing the roughness inside
7 the hollows and the height distribution within the **Fe₄Ph** layer, respectively.
8
9

10
11
12
13
14
15
16
17
18 In order to get a deeper insight, the interaction of **Fe₄Ph** with the Au(111) surface was
19 investigated by a periodic-DFT approach based on the revPBE functional²⁸ plus D3 dispersion
20 corrections²⁹ (see SI for details). The optimized structure of **Fe₄Ph** adsorbed on the metal is
21 reported in Fig 1b. The molecule revealed to be rigid enough to keep its core geometry almost
22 unchanged, as it is evident from Fig. 1b, with changes which do not exceed one degree for the
23 average Fe-O-Fe bridging angle (see Table S4.2). The easy axis of the magnetization, taken as
24 the normal to the plane containing the four iron ions, was evaluated to form an angle of 34.4°
25 with the normal to the surface. This value is close to the one found for a thioacetyl functionalized
26 analogue, chemically grafted to the Au(111) surface.²⁴ We notice that the physisorption energy
27 of **Fe₄Ph** (40.3 kcal mol⁻¹) is due mainly to the large number of favorable Au-H interactions,
28 whose contribution is however expected to be overestimated by the employed D3 energy
29 dispersion corrections.²⁹
30
31
32
33
34
35
36
37
38
39
40
41
42
43
44
45

46 On the basis of the DFT optimized structure it has been possible to simulate (Fig. 2e) an STM
47 image of the **Fe₄Ph** molecule on Au(111). Due to the low conductivity of the ligands shell a
48 quasi-spherical multi-lobed structure is visible in line with experiment, though the sub-molecular
49 resolution is much poorer than for flat molecules like TbPc₂. An average diameter of *ca.* 1.9 nm
50 can be estimated from the computed image, in agreement with the experimental STM values.
51
52
53
54
55
56
57
58
59
60

1
2
3 As far as the magnetic properties of **Fe₄Ph** adsorbed on gold are concerned, the evaluation of
4 its magnetic structure was performed using the well-established Broken Symmetry (BS)
5 formalism^{30,31} within the DFT framework and developing the approach reported in ref.³² Such an
6 approach allows to estimate the value of the exchange-coupling constants in the spin
7 Hamiltonian:
8
9
10
11
12
13

$$H_{ex} = J_1(\mathbf{S}_1 \cdot \mathbf{S}_2 + \mathbf{S}_1 \cdot \mathbf{S}_3 + \mathbf{S}_1 \cdot \mathbf{S}_4) + J_2(\mathbf{S}_2 \cdot \mathbf{S}_3 + \mathbf{S}_3 \cdot \mathbf{S}_4 + \mathbf{S}_2 \cdot \mathbf{S}_4) \quad \text{eq. 1}$$

14
15
16
17
18
19

20 where threefold symmetry is assumed and J_1 and J_2 account for nearest-neighbor and next-
21 nearest neighbor interactions, respectively. A spin Hamiltonian with lower symmetry was also
22 tested (see Table S4.1 and SI for more details) resulting however in negligible deviations from
23 threefold symmetry.
24
25
26
27
28
29

30 It is well known that the inclusion of Hartree-Fock (HF) exchange by using hybrid functional
31 is necessary to accurately evaluate magnetic interactions.³³ We applied first this approach, using
32 the PBE0 functionals,³⁴ to the optimized geometries of **Fe₄Ph** molecules in the gas phase and
33 adsorbed on gold. However, in the latter case the entire system is computationally too demanding
34 at this level of approach. The exchange coupling constants for the adsorbed scenario were thus
35 computed only on the geometry of the cluster already optimized on the gold surface at the
36 revPBE level on the extrapolated geometry, *i.e.* removing the gold surface without any further
37 relaxation.
38
39
40
41
42
43
44
45
46
47
48

49 The results reported in Table 1 show minor changes in the magnetic coupling constants, as
50 expected from the small modifications observed in the molecular geometry upon adsorption.
51
52
53
54
55
56
57
58
59
60

Table 1: J values (in cm^{-1}) computed on experimental and optimized **Fe₄Ph** geometries with different approaches. U values for all atomic species except Au^a are taken from ref.³⁵

	PBE0			revPBE+U		
	J_1	J_2	$\Delta E_{5,4}^b$	J_1	J_2	$\Delta E_{5,4}^b$
Fe₄Ph (X-ray structure)	14.4	0.3	34	17.0	0.4	40
Fe₄Ph (Optimized structure)	13.8	0.2	33	16.7	0.3	40
Fe₄Ph@Au (Extrapolated)	14.7	0.1	36	17.9	0.2	43
Fe₄Ph@Au ^a	-	-	-	15.0÷18.8	0.31÷-1.2	35÷56
Experimental	16.37(12)	0.29(11)	42			

^a Computed adding a $U_{\text{Au}5d}$ value which varies from 0 to 0.6 eV. The chosen range is the one compatible with the Au(111) UPS spectrum. The corresponding ranges of computed J_1 , J_2 , $\Delta E_{5,4}$ values are reported (see SI for more details).^b Energy gap between the ground $S = 5$ and the two first-excited $S = 4$ states.

In order to investigate the whole molecule-plus-substrate system (**Fe₄Ph@Au**), without losing the accuracy achievable with hybrid functional, we employed a less demanding approach, based on an alternative parametric method, DFT+U.^{36,37} In this framework a HF-like potential (U) describing the interaction between electrons localized on the same center (on-site interactions) was introduced. The choice of the U parameters is critical for a correct description of the electronic structure, and the values employed here were previously optimized by reproducing both the magnetic properties and the experimental valence band structure of **Fe₄Ph** obtained by Ultraviolet Photoelectron Spectroscopy (UPS).³⁵ The magnetic interactions computed at the revPBE+U level, reported in Table 1, confirm that the overall scenario of a dominant antiferromagnetic J_1 interaction is preserved, with a ground state $S = 5$ separated by $35\div 56 \text{ cm}^{-1}$ from the excited $S = 4$ states, depending on the chosen $U_{\text{Au}5d}$ parameter. The results for the

1
2
3 complex **Fe₄Ph@Au** system indicate only minor effects induced by the interaction with the
4 substrate. Interestingly, both approaches employed here (the extrapolated molecule from the
5 surface and the full system treated at DFT+U level) confirm substantial conservation of
6 intramolecular antiferromagnetic coupling upon grafting. In details a slight increase of the $\Delta E_{5,4}$
7 is expected when larger $U_{\text{Au}5d}$ values are considered. The magnetic anisotropy, not included in
8 our treatment, is also not expected to vary significantly due to the minor geometrical
9 modifications and almost negligible electronic effects arising from the proximity of the metallic
10 substrate.
11
12

22 Experimental insight into the electronic structure and magnetic behavior of surface-supported
23 **Fe₄Ph** SMMs sub-monolayer was obtained through synchrotron-based X-ray absorption
24 techniques, a key tool for investigation of thin deposits of magnetic molecules.^{38,39} Surface
25 selectivity and sensitivity to submonolayer coverages is in fact achieved by measuring the
26 absorption in the Total Electron Yield (TEY) mode,⁴⁰ which is based on the emission of
27 secondary electrons and the detection of the current flow to re-establish neutrality. Moreover, X-
28 ray absorption based experiments involve core orbitals and are element and oxidation-state
29 selective. Finally, by employing circularly polarized light with opposite helicities and measuring
30 the absorption with right (σ^-) and left (σ^+) polarized light (see SI), X-ray Magnetic Circular
31 Dichroism (XMCD) is evaluated as $\sigma^- - \sigma^+$, thus obtaining information on the magnetic moment
32 at the probed atoms.
33
34
35
36
37
38
39
40
41
42
43
44
45
46
47

48 A submonolayer of **Fe₄Ph**, *ca.* 0.5 ML, thus intermediate between the two coverages studied
49 by STM, was sublimated *in-situ* and investigated using synchrotron radiation (see SI). The XAS
50 spectra recorded at the Fe L_{2,3} edge on a submonolayer of **Fe₄Ph** on Au (Fig.1c) are typical for
51 this class of propeller-like complexes⁴¹ suggesting that the contaminant domains are mainly
52
53
54
55
56
57
58
59
60

1
2
3 formed by metal-free organic fragments. The amplitude and shape of the XMCD signal, with a
4 vanishing response in between the two main peaks of the L_3 edge (707.9 eV), are also similar to
5 those found in other derivatives,⁴¹ either as bulk phases or chemisorbed on gold. They have been
6 associated to the ferrimagnetic spin arrangement in the ground $S = 5$ state and are therefore
7 diagnostic of intact **Fe₄Ph** molecules.^{19,42,43}

8
9
10 The ^3He - ^4He dilution cryostat⁴⁴ available at the beamline allowed to reach sub-kelvin
11 temperatures and to record magnetic hysteresis curves by monitoring the field dependence of the
12 XMCD signal at the energy of its maximum (709.1 eV). The results obtained at three different
13 temperatures are reported in Fig. 4. The measurement at the lowest accessible temperature (0.68
14 K) was carried out at two different orientations of the magnetic field with respect to the surface
15 normal, *i.e.* $\theta = 0^\circ$ and 45° (see inset of Fig.1c for a scheme of the experiment). The temperature
16 dependence is in line with previous measurements on bulk as well as chemisorbed SMMs of the
17 same family.^{42,43} A butterfly shaped hysteresis loop is recovered at this temperature with well-
18 defined steps around zero field and ± 5 kOe. An important feature is that the observed step
19 positions for $\theta = 0^\circ$ are in good agreement with those expected for resonant quantum tunneling
20 of the magnetization (QTM)³ when the magnetic field is applied along the easy axis (z), *i.e.* $|H_1|$
21 $= |D|/(g\mu_B) = 4.5$ kOe. Furthermore, the steps shift to higher field on increasing the θ angle.
22 Finally, the XMCD signal at $\theta = 0^\circ$ levels off at low field, while a more gradual increase at
23 higher fields is observed for $\theta = 45^\circ$. A similar behavior was previously found in a monolayer of
24 a sulfur-functionalized Fe_4 derivative²⁴ and attributed to a preferential grafting of the molecules
25 with their easy axis perpendicularly to the surface. Such a partial ordering of **Fe₄Ph** molecules is
26 in line with our *ab initio* calculations presented above.

1
2
3 We also directly probed the time dependence of the magnetization at 0.68 K by first
4 magnetizing the system in a +16 kOe magnetic field, fast sweeping the field to -2.5 kOe and then
5 monitoring the time evolution of the XMCD signal at 709.1 eV. This particular field was chosen
6 as it lies in between the resonant QTM steps and consequently affords the slowest magnetic
7 relaxation. Notice that in zero-field the magnetization dynamics is too fast to be measured by
8 XMCD and, additionally, the signal/noise response of the TEY detector becomes much worse.
9
10 The investigation has been carried out at both θ angles and the characteristic time of the decay,
11 *i.e.* 1400 ± 100 s and 1100 ± 100 s for $\theta = 0^\circ$ and $\theta = 45^\circ$, respectively, has been evaluated by
12 fitting the experimental data to a mono-exponential law.
13
14

15
16 Following a previously developed approach, we used quantum master matrix²⁴ calculations to
17 reproduce the temperature and angular dependence of the hysteresis curves reported in Fig. 4.
18 This numerical approach allows to take into account a preferential orientation of the molecules
19 on the surfaces. Though the spin Hamiltonian parameters previously employed to describe axial
20 and transverse anisotropy provided a reasonable agreement with the experimental data, the sixth-
21 order transverse term, very efficient in promoting QTM at low temperature, was added in
22 agreement with spectroscopic evidences.⁴⁵ An acceptable agreement was obtained with $D/k_B = -$
23 0.6 K, $E/k_B = 0.02$ K, $B_4^3/k_B = 0.005$ K and $B_6^6/k_B = 3 \times 10^{-6}$ K, where E embodies the second-
24 order rhombic anisotropy, and the last two terms describe fourth and sixth-order transverse
25 anisotropies that are relevant in Fe_4 complexes.^{3,45,46} The inclusion of a sixth-order term allowed
26 to significantly reduce the other transverse terms compared to previous simulations, though they
27 are still larger than those observed for similar derivatives in the crystalline phase.⁴⁵ Moreover the
28 easy magnetic axes were restricted to be randomly distributed within the angular range $30^\circ - 40^\circ$
29 from the surface normal, as suggested by DFT calculations. An additional contribution of 20%
30
31
32
33
34
35
36
37
38
39
40
41
42
43
44
45
46
47
48
49
50
51
52
53
54
55
56
57
58
59
60

randomly-oriented molecules was introduced as the magnetization does not achieve full saturation.

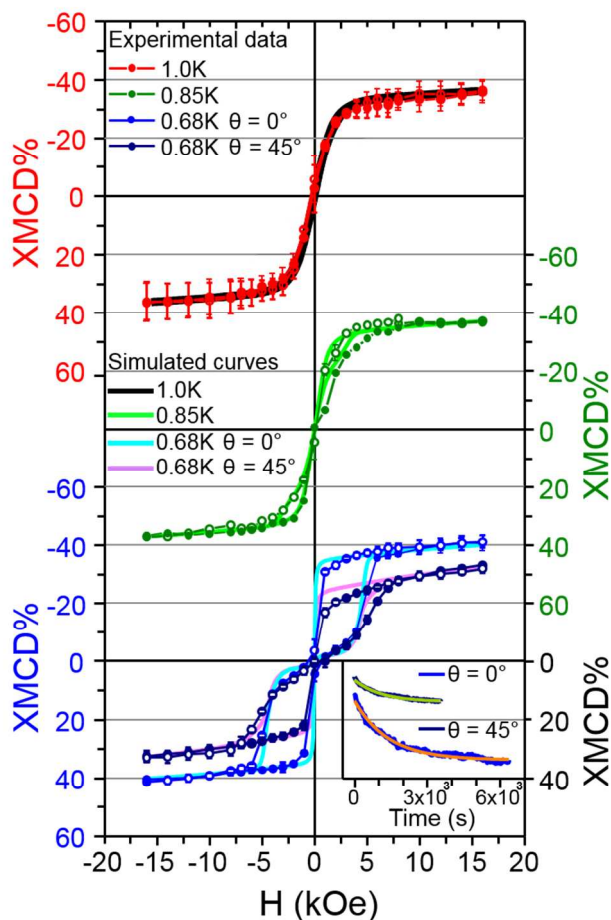


Figure 4. Temperature-dependent hysteresis loops acquired by monitoring the field dependence of the XMCD signal at 709.1 eV; at the lowest temperature the hysteresis loop has been measured at $\theta = 0^\circ$ (blue) and $\theta = 45^\circ$ (dark blue). Data recorded with decreasing field indicated as empty symbols. Each experimental hysteresis loop is superimposed to the calculated one. The acquisition of a full hysteresis loop required *ca.* 90 min. The inset presents time decay data recorded at -2.5 kOe after saturation at +16 kOe; the solid lines are fits to a mono-exponential law (green $\theta = 45^\circ$ and orange $\theta = 0^\circ$); data are expressed in the same reference scale as the hysteresis loops.

1
2
3
4
5
6
7
8
9
10
11
12
13
14
15
16
17
18
19
20
21
22
23
24
25
26
27
28
29
30
31
32
33
34
35
36
37
38
39
40
41
42
43
44
45
46
47
48
49
50
51
52
53
54
55
56
57
58
59
60

Though the strong correlation between parameters prevented the determination of a unique set of spin Hamiltonian parameters, the good agreement with experimental data at this level of approximation further confirms that Fe_4Ph is able to retain its SMM properties at the submonolayer level. It is interesting to notice that magnetization jumps at resonant fields ($H = 0$ and ± 5 kOe) occur in a narrower field range in calculated hysteresis loops than in the experimental ones. This discrepancy could arise from neglecting local dipolar fields in our simulation. In a three-dimensional (3D) crystal of magnetically-saturated molecules, the magnitude and orientation of local dipolar fields are crucially dependent on the crystal structure. By contrast, in a bidimensional (2D) lattice of molecules magnetized perpendicular to the surface (say, along $-Z$), the local dipolar fields are always oriented antiparallel to the magnetizing field (*i.e.* along $+Z$). Furthermore, since dipolar contributions from all sites sum up constructively, dipolar fields can easily exceed those typical of 3D arrays. Sample calculations assuming a hexagonal 2D lattice with 1.6 nm spacing between $S=5$ spins reveal a dipolar bias of *ca.* 24 mT, hence significantly larger than for a related 3D crystal.⁴⁷ Peculiar is also the evolution of local dipolar fields during magnetic relaxation (“dipolar shuffling”).⁴⁸ After the system is initialized with all magnetic moments along $-Z$ (lower left branch of the hysteresis loop in Fig. 4), spin reversal is expected to start at a slightly negative H value due to the positive dipolar bias. Because reversing some spins diminishes the dipolar bias on the array, the remaining spins will have additional possibilities to flip at higher H values, *i.e.* later in the sweep. Though a quantitative analysis is beyond the scope of this work, such “dipolar shuffling” effects are predicted to broaden magnetization steps and, in addition, to favor relaxation. The evolution of dipolar fields can indeed explain why oriented 2D arrays of SMMs display no remnant magnetization and a more pronounced tunneling, thus justifying why larger transverse anisotropy

1
2
3 terms are necessary to simulate their hysteresis loop. We anticipate here that a more pronounced
4
5 bistability may result for isolated SMMs on a surface as compared with a densely-packed
6
7 monolayer.
8
9

10 In summary, through a combined morphological and spectroscopic characterization we
11 demonstrated here that **Fe₄Ph** SMMs can be sublimated on gold with layer-by-layer growth of
12 partially-oriented molecules. More importantly, we showed that at submonolayer coverage the
13 magnetic bistability of the magnetization is preserved after this UHV-based deposition approach
14 with enhanced tunneling due to the bidimensional arrangement of the SMMs. These findings
15 suggest a weak interaction with the gold substrate that was confirmed by state-of-the-art first
16 principles calculations.
17
18
19
20
21
22
23
24
25

26 Even though a detailed *in-situ* characterization has evidenced the unavoidable co-presence of
27 contaminants, such deposition conditions are suitable to address intact and isolated molecules by
28 STM methods. Furthermore, they open the perspective of assembling in UHV conditions
29 molecular-inorganic hybrid architectures that can be useful in spintronic devices.
30
31
32
33
34
35
36
37

38 ASSOCIATED CONTENT

39
40
41 XPS calibration of molecular film thickness, series of STM supporting images; information on
42 the XAS and XMCD experimental procedures; computation details. This material is available
43 free of charge via the Internet at <http://pubs.acs.org>
44
45
46
47
48
49

50 AUTHOR INFORMATION

51 **Corresponding Author**

52
53
54
55
56
57
58
59
60

1
2
3 * (R.S.) roberta.sessoli@unifi.it
4
5
6

7 **Author Contributions**

8
9
10 The manuscript was written through contributions of all authors.
11
12

13 14 15 16 **ACKNOWLEDGMENT**

17
18
19 We acknowledge the financial contribution of the European Research Council through the
20
21 Advanced Grant MolNanoMaS (267746), of Italian MIUR through FIRB project
22
23 RBAP117RWN, and of CINECA through the ISCRA initiative. The support of the EC through the
24
25 FP7/2007-2013 Calypso project (n° 31228) and of Ente Cassa di Risparmio di Firenze is also
26
27 acknowledged.
28
29
30

31
32 We thank L. Joly, J.-P. Kappler, B. Muller, and F. Scheurer for their contribution in installing
33
34 the IMPMC-IPCMS-SOLEIL dilution refrigerator. We acknowledge SIM staff for the beamline
35
36 management. We also thank the CINECA award under the ISCRA initiative, for the availability
37
38 of high performance computing resources and support.
39
40
41

42 43 44 **REFERENCES**

- 45
46 (1) Thomas, L.; Lioni, F.; Ballou, R.; Gatteschi, D.; Sessoli, R.; Barbara, B. *Nature* **1996**,
47
48 *383*, 145–147.
49
50
51
52 (2) Friedman, J.; Sarachik, M.; Tejada, J.; Ziolo, R. *Phys. Rev. Lett.* **1996**, *76*, 3830–3833.
53
54
55
56
57
58
59
60

- 1
2
3 (3) Gatteschi, D.; Sessoli, R.; Villain, J. *Molecular Nanomagnets*; Oxford University Press,
4 Ed.; Oxford, 2006.
5
6
7
8
9 (4) Bogani, L.; Wernsdorfer, W. *Nat. Mater.* **2008**, *7*, 179–186.
10
11
12 (5) Komeda, T.; Isshiki, H.; Liu, J.; Zhang, Y.-F.; Lorente, N.; Katoh, K.; Breedlove, B. K.;
13 Yamashita, M. *Nat. Commun.* **2011**, *2*, 217.
14
15
16
17 (6) Schwöbel, J.; Fu, Y.; Brede, J.; Dilullo, A.; Hoffmann, G.; Klyatskaya, S.; Ruben, M.;
18 Wiesendanger, R. *Nat. Commun.* **2012**, *3*, 953.
19
20
21
22
23 (7) Fu, Y.-S.; Schwöbel, J.; Hla, S.-W.; Dilullo, A.; Hoffmann, G.; Klyatskaya, S.; Ruben,
24 M.; Wiesendanger, R. *Nano Lett.* **2012**, *12*, 3931–3935.
25
26
27
28
29 (8) Jo, M.-H.; Grose, J. E.; Baheti, K.; Deshmukh, M. M.; Sokol, J. J.; Rumberger, E. M.;
30 Hendrickson, D. N.; Long, J. R.; Park, H.; Ralph, D. C. *Nano Lett.* **2006**, *6*, 2014–2020.
31
32
33
34 (9) Burzurí, E.; Yamamoto, Y.; Warnock, M.; Zhong, X.; Park, K.; Cornia, A.; van der Zant,
35 H. S. J. *Nano Lett.* **2014**, *14*, 3191-3196..
36
37
38
39 (10) Barraza-Lopez, S.; Park, K.; García-Suárez, V.; Ferrer, J. *Phys. Rev. Lett.* **2009**, *102*,
40 246801.
41
42
43
44 (11) Urdampilleta, M.; Klyatskaya, S.; Cleuziou, J.-P.; Ruben, M.; Wernsdorfer, W. *Nat.*
45 *Mater.* **2011**, *10*, 502–506.
46
47
48
49 (12) Vincent, R.; Klyatskaya, S.; Ruben, M.; Wernsdorfer, W.; Balestro, F. *Nature* **2012**, *488*,
50 357–360.
51
52
53
54
55
56
57
58
59
60

1
2
3 (13) Zyazin, A. S.; van den Berg, J. W. G.; Osorio, E. A.; van der Zant, H. S. J.;
4 Konstantinidis, N. P.; Leijnse, M.; Wegewijs, M. R.; May, F.; Hofstetter, W.; Danieli, C.;
5 Cornia, A. *Nano Lett.* **2010**, *10*, 3307–3311.
6
7
8

9
10
11 (14) Ishikawa, N.; Sugita, M.; Tanaka, N.; Ishikawa, T.; Koshihara, S.; Kaizu, Y. *Inorg.*
12 *Chem.* **2004**, *43*, 5498–5500.
13
14

15
16
17 (15) Gonidec, M.; Biagi, R.; Corradini, V.; Moro, F.; De Renzi, V.; del Pennino, U.; Summa,
18 D.; Muccioli, L.; Zannoni, C.; Amabilino, D. B.; Veciana, J. *J. Am. Chem. Soc.* **2011**, *133*, 6603–
19 6612.
20
21
22

23
24
25 (16) Klar, D.; Candini, A.; Joly, L.; Klyatskaya, S.; Krumme, B.; Ohresser, P.; Kappler, J.-P.;
26 Ruben, M.; Wende, H. *Dalton Trans.* **2014**, *43*, 10686–10689.
27
28

29
30 (17) Mannini, M.; Bertani, F.; Tudisco, C.; Malavolti, L.; Poggini, L.; Misztal, K.; Menozzi,
31 D.; Motta, A.; Otero, E.; Ohresser, P.; Sainctavit, Ph.; Condorelli, G. G.; Dalcanale, E.; Sessoli,
32 R. *Nat. Commun.* **2014**, *5*, 4582.
33
34
35

36
37
38 (18) Stepanow, S.; Honolka, J.; Gambardella, P.; Vitali, L.; Abdurakhmanova, N.; Tseng, T.-
39 C.; Rauschenbach, S.; Tait, S. L.; Sessi, V.; Klyatskaya, S.; Ruben, M.; Kern, K. *J. Am. Chem.*
40 *Soc.* **2010**, *132*, 11900–11901.
41
42
43

44
45
46 (19) Margheriti, L.; Chiappe, D.; Mannini, M.; Car, P.-E.; Sainctavit, Ph.; Arrio, M.-A.; de
47 Mongeot, F. B.; Cezar, J. C.; Piras, F. M.; Magnani, A.; Otero, E.; Caneschi, A.; Sessoli, R. *Adv.*
48 *Mater.* **2010**, *22*, 5488–5493.
49
50
51

1
2
3 (20) Lodi Rizzini, A.; Krull, C.; Balashov, T.; Kavich, J. J.; Mugarza, A.; Miedema, P. S.;
4 Thakur, P. K.; Sessi, V.; Klyatskaya, S.; Ruben, M.; Stepanow, S.; Gambardella, P. *Phys. Rev.*
5
6
7
8 *Lett.* **2011**, *107*, 177205.

9
10
11 (21) Lodi Rizzini, A.; Krull, C.; Balashov, T.; Mugarza, A.; Nistor, C.; Yakhou, F.; Sessi, V.;
12
13 Klyatskaya, S.; Ruben, M.; Stepanow, S.; Gambardella, P. *Nano Lett.* **2012**, *12*, 5703–5707.

14
15
16 (22) Malavolti, L.; Poggini, L.; Margheriti, L.; Chiappe, D.; Graziosi, P.; Cortigiani, B.;
17
18 Lanzilotto, V.; de Mongeot, F. B.; Ohresser, P.; Otero, E.; Choueikani, F.; Saintavit, Ph.;
19
20 Bergenti, I.; Dediu, V. A.; Mannini, M.; Sessoli, R. *Chem. Commun.* **2013**, *49*, 11506–11508.

21
22 (23) Mannini, M.; Pineider, F.; Saintavit, Ph.; Danieli, C.; Otero, E.; Sciancalepore, C.;
23
24
25 Talarico, A. M.; Arrio, M.-A.; Cornia, A.; Gatteschi, D.; Sessoli, R. *Nat. Mater.* **2009**, *8*, 194–
26
27
28
29
30
31 197.

32
33 (24) Mannini, M.; Pineider, F.; Danieli, C.; Totti, F.; Sorace, L.; Saintavit, Ph.; Arrio, M.-A.;
34
35 Otero, E.; Joly, L.; Cezar, J. C.; Cornia, A.; Sessoli, R. *Nature* **2010**, *468*, 417–421.

36
37
38 (25) Margheriti, L.; Mannini, M.; Sorace, L.; Gorini, L.; Gatteschi, D.; Caneschi, A.; Chiappe,
39
40
41 D.; Moroni, R.; de Mongeot, F. B.; Cornia, A.; Piras, F. M.; Magnani, A.; Sessoli, R. *Small*
42
43
44
45 **2009**, *5*, 1460–1466.

46
47 (26) Rigamonti, L.; Piccioli, M.; Malavolti, L.; Poggini, L.; Mannini, M.; Totti, F.; Cortigiani,
48
49
50 B.; Magnani, A.; Sessoli, R.; Cornia, A. *Inorg. Chem.* **2013**, *52*, 5897–5905.

51
52 (27) The dimension has been estimated as the largest intramolecular distance, corresponding
53
54
55 to a pair of H atoms of the *dpm* ligands, increased by the corresponding Van der Waals radii.

56
57 (28) Zhang, Y.; Yang, W. *Phys. Rev. Lett.* **1998**, *80*, 890.
58
59
60

- 1
2
3 (29) Grimme, S.; Antony, J.; Ehrlich, S.; Krieg, H. *J. Chem. Phys.* **2010**, *132*, 154104.
4
5
6 (30) Noodleman, L.; Norman, J. G. *J. Chem. Phys.* **1979**, *70*, 4903.
7
8
9 (31) Noodleman, L. *J. Chem. Phys.* **1981**, *74*, 5737.
10
11
12 (32) Totti, F.; Rajaraman, G.; Iannuzzi, M.; Sessoli, R. *J. Phys. Chem. C* **2013**, *117*, 7186–
13 7190.
14
15
16 (33) Adamo, C.; Barone, V.; Bencini, A.; Totti, F.; Ciofini, I. *Inorg. Chem.* **1999**, *38*, 1996–
17 2004.
18
19 (34) Adamo, C.; Barone, V. *J. Chem. Phys.* **1999**, *110*, 6158.
20
21
22 (35) Ninova, S.; Lanzilotto, V.; Malavolti, L.; Rigamonti, L.; Cortigiani, B.; Mannini, M.;
23 Totti, F.; Sessoli, R. *J. Mater. Chem. C* **2014**, in press. doi:10.1039/C4TC01647E.
24
25
26 (36) Anisimov, V. I.; Zaanen, J.; Andersen, O. K. *Phys. Rev. B* **1991**, *44*, 943–954.
27
28
29 (37) Cococcioni, M.; de Gironcoli, S. *Phys. Rev. B* **2005**, *71*, 035105.
30
31
32 (38) Cornia, A.; Mannini, M. *Structure and Bonding*; Springer Berlin Heidelberg, 2014; pp. 1–
33 38.
34
35
36 (39) Sessoli, R.; Mannini, M.; Pineider, F.; Cornia, A.; Sainctavit, P. In *Magnetism and*
37 *synchrotron radiation*; Springer, Ed.; Berlin, 2010; pp. 279–311.
38
39
40 (40) Nakajima, R.; Stöhr, J.; Idzerda, Y. *U. Phys. Rev. B* **1999**, *59*, 6421–6429.
41
42
43
44
45
46
47
48
49
50
51
52
53
54
55
56
57
58
59
60

1
2
3 (41) Mannini, M.; Pineider, F.; Saintavit, Ph.; Joly, L.; Fraile-Rodríguez, A.; Arrio, M.-A.;
4
5 Cartier dit Moulin, C.; Wernsdorfer, W.; Cornia, A.; Gatteschi, D.; Sessoli, R. *Adv. Mater.* **2009**,
6
7 *21*, 167–171.
8
9

10
11 (42) Accorsi, S.; Barra, A.-L.; Caneschi, A.; Chastanet, G.; Cornia, A.; Fabretti, A. C.;
12
13 Gatteschi, D.; Mortalo, C.; Olivieri, E.; Parenti, F.; Rosa, P.; Sessoli, R.; Sorace, L.;
14
15 Wernsdorfer, W.; Zobbi, L. *J. Am. Chem. Soc.* **2006**, *128*, 4742–4755.
16
17

18
19 (43) Cornia, A.; Fabretti, A. C.; Garrisi, P.; Mortalò, C.; Bonacchi, D.; Gatteschi, D.; Sessoli,
20
21 R.; Sorace, L.; Wernsdorfer, W.; Barra, A.-L. *Angew. Chem. Int. Ed. Engl.* **2004**, *43*, 1136–1139.
22
23

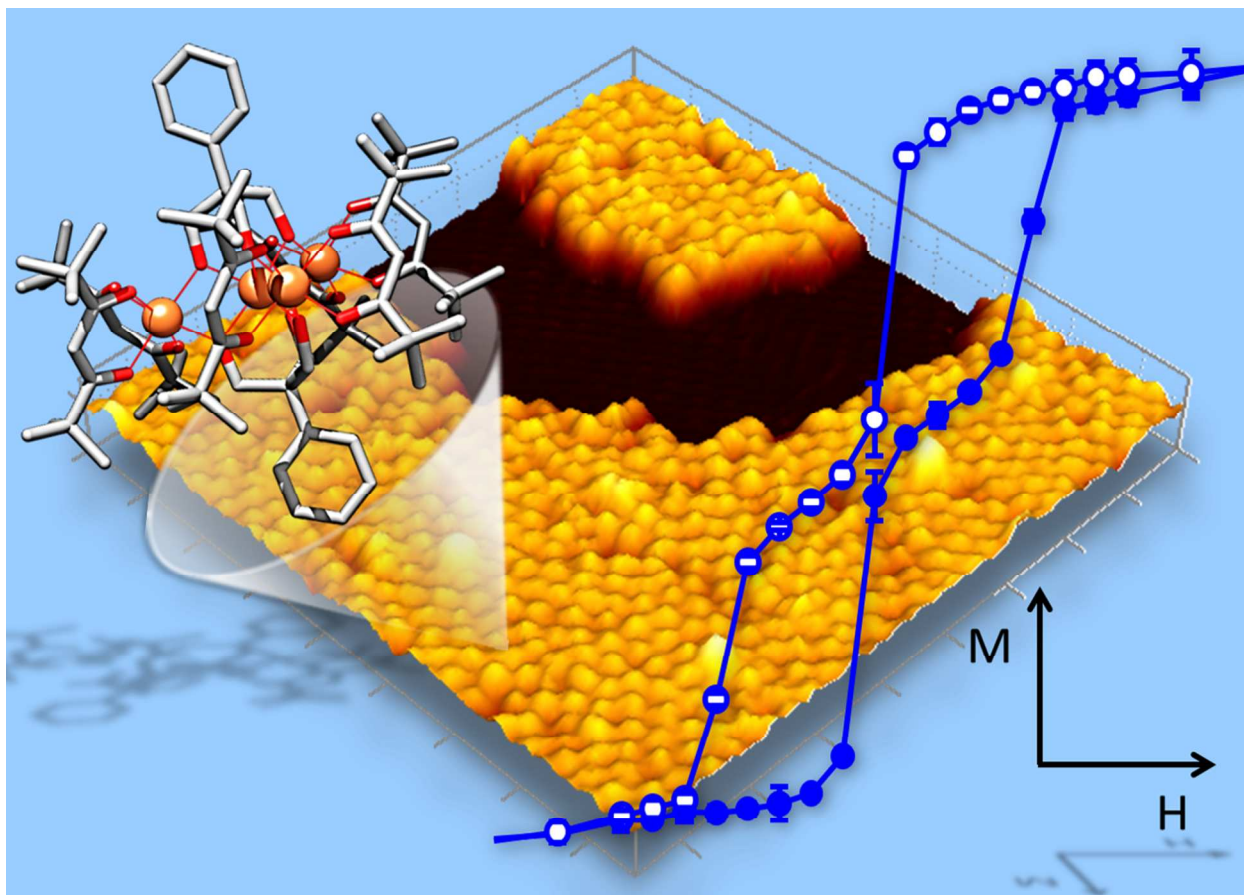
24
25 (44) Letard, I.; Saintavit, Ph.; dit Moulin, C. C.; Kappler, J.-P.; Ghigna, P.; Gatteschi, D.;
26
27 Doddi, B. *J. Appl. Phys.* **2007**, *101*, 113920.
28
29

30
31 (45) Sorace, L.; Boulon, M.-E.; Totaro, P.; Cornia, A.; Fernandes-Soares, J.; Sessoli, R. *Phys.*
32
33 *Rev. B* **2013**, *88*, 104407.
34
35

36 (46) Abragam, A.; Bleaney, B. *Electron Paramagnetic Resonance of Transition Ions*; S, Ed.;
37
38 Dover: New York, 1986.
39
40

41 (47) Vergnani, L.; Barra, A.-L.; Neugebauer, P.; Rodriguez-Douton, M. J.; Sessoli, R.; Sorace,
42
43 L.; Wernsdorfer, W.; Cornia, A. *Chemistry* **2012**, *18*, 3390–3398.
44
45

46
47 (48) Liu, J.; Wu, B.; Fu, L.; Diener, R.; Niu, Q. *Phys. Rev. B* **2002**, *65*, 224401.
48
49
50
51
52
53
54
55
56
57
58
59
60



1
2
3
4
5
6
7
8
9
10
11
12
13
14
15
16
17
18
19
20
21
22
23
24
25
26
27
28
29
30
31
32
33
34
35
36
37
38
39
40
41
42
43
44
45
46
47
48
49
50
51
52
53
54
55
56
57
58
59
60